High-throughput Robotic Phenotyping of Energy Sorghum Crops

Srinivasan Vijayarangan, Paloma Sodhi, Prathamesh Kini, James Bourne, Simon Du, Hanqi Sun, Barnabas Poczos, Dimitrios Apostolopoulos, and David Wettergreen

Abstract Plant phenotyping is a time consuming, labour intensive, error prone process of measuring the physical properties of plants. We present a scalable robotic system which employs computer vision and machine learning to phenotype plants rapidly. It maintains high throughput making multiple phenotyping measurements during the plant lifecycle in plots containing thousands of plants. Our novel approach allows scanning of plants inside the plant canopy in addition to the top and bottom section of the plants. Here we present our design decisions, implementation challenges and field observations.

1 Introduction

Biofuels are a significant source of renewable energy. However, only limited amounts of biofuels are produced from non-grain feedstocks because production costs are not competitive. Increased yield of bioenergy crops would mitigate this barrier to utilization. While crop breeding and improved management practices have increased productivity, the rate of yield gain in most crops is 1-2% per year with very significant investment. The ability to correlate phenotypic traits with their genotypes plays a crucial role in improving plant breeding techniques. Phenotyping is the bottleneck in the plant breeding pipeline and high throughput automated methods are crucial to improved production [1], [2]. We have created our high-throughput robotic phenotyping system which is capable of measuring a comprehensive set of phenotypes associated with traits that impact biomass yield with high accuracy and repeatability.

Plant phenotyping is the quantitative assessment of plant traits like physiology, yield, etc. Currently, plant phenotyping is a manually intensive, slow, error prone process which involves humans making measurements in the field or greenhouse. In most cases, the phenotyped data is analyzed post-season. However with our high-

Srinivasan Vijayarangan
Carnegie Mellon University e-mail: srinivasan@cmu.edu

Fig. 1: High-throughput Phenotyping robot in a sorghum field in Weslaco, Texas. Sorghum grows 6 meters tall in 4 months.

throughput system, we can collect plant phenotype data much faster and accurately. We can also collect more measurements compared to the current manual methods, which helps to increase the accuracy and completeness of the estimates. Unlike some manual methods, our system is non intrusive which means we can scan the plant multiple times during its life cycle and not affect its development. Energy sorghum is used in this program because it is a highly productive, annual, drought tolerant C4 grass with an excellent genetic (diploid, inbreeding) and genomics platform [3], [4].

Our main contribution is the design and development of a high throughput plant phenotyping robot which was deployed in the field to measure phenotype traits associated with energy crop traits that impact biomass yield, with high precision and reproducibility. Its novel properties are:

1. Capable of plunging its sensor boom into the plant canopy to measure traits not visible from above or below without damaging the plants which enables multiple measurement during the life-cycle of the plant.
2. A system capable of handling the large-scale data processing, feature extraction, plant modeling and phenotype estimation.

2 Related Work

2.1 High-Throughput Phenotyping Platforms

Field phenotyping platforms include ground-based and aerial-based methods [12]. Aerial-based platforms enable greater coverage and rapid characterization of field plots, but are limited in spatial resolution and payload capacity. They are more suitable for estimating macro-phenotypic traits like plant location and densities [20].

Ground-based platforms can yield more detailed phenotypic information at the cost of relatively lower coverage rates. Lemnatec is one of the leaders in automated phenotyping with in-field platforms like Bonirob [22] and Scanalyzer Field [21]. Bonirob is an autonomous field robot designed to be a reusable platform for multiple agricultural applications like phenotyping, precision spraying and penetrometer measurement [22]. The Scanalyzer Field is an overhead gantry system with a sensor payload constituting imaging systems like fluroscence imaging, multi-spectral cameras and LiDAR [21]. While the Bonirob is a mobile platform capable of navigating between crop rows, the Scanalyzer Field is a gantry system on rails limited to small sites in which it can operate. Both platforms, however, are overhead phenotyping systems limited to top-down views of the plant and unable to see into closed canopy. This paper describes a mobile tractor-based phenotyping platform capable of collecting plant images at multiple vertical and horizontal viewpoints inside the closed plant canopy.

2.2 Plant Imaging and Phenotype Estimation

High-throughput phenotyping platforms deploy a variety of imaging modalities like 2D visible imaging, 3D imaging, multispectral imaging, thermal infrared imaging and fluorescence imaging [12]. Given its low cost and ease of operation, 2D/3D visible imaging has been commonly used for applications like plant mapping and detection [13], weed control [14], fruit counting and yield estimation [17]. For the purpose of phenotyping, the use of 3D visible imaging is important in order to be able to make ground truth metric measurements purely from imaging. However, most of the current state-of-the-art in 3D plant reconstruction, segmentation and phenotyping is in controlled greenhouse environments [18], [7], [19]. This paper demonstrates results for in-field 3D reconstruction and segmentation of plant structures from imaging data collected by the phenotyping platform. It compares these against reconstructions obtained from a greenhouse environment, and also proposes preliminary phenotype estimation methods on the greenhouse data.

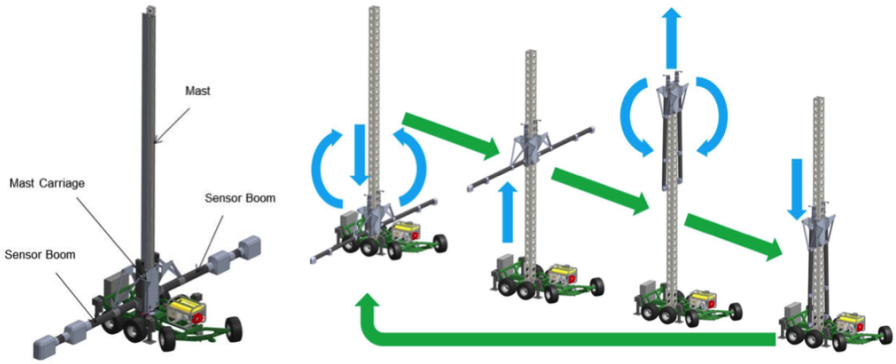

Fig. 2: High-throughput Phenotyping Robot - (a) trailer with the sensorpod (b) deployment sequence showing arms carrying sensorpods stretched out at the bottom; followed by sweeping up motion inside plant canopy; and finally folding back into the mast

3 High-throughput Phenotyping Robot

The robot resides on a trailer system that provides an inexpensive support and transport system for the sensor boom and mast. The trailer will move in the alley ways between sub plots and once in position, drop leveling legs to stabilize the mast so that the sensor boom can be deployed reliably.

The trailer is a six-wheeled vehicle with *bogie* suspension. This type of suspension provides for a certain amount of terrain averaging without requiring a spring/damper-type suspension system. Hubs, axles, tires, wheels, trailer coupler and stabilizing jack (auto leveling) system are all commercial off- the-shelf items. The total weight of the system is $\sim$1000 kg including the mast and sensor boom. The overall footprint of the trailer is 1.5m wide by 3m long. The solid front axle pivots for steering, providing an approximate 2.5m turning radius. This vehicle requires an alley way of 1.8m.

The system consists of a vertical column carrying opposing sensor booms as shown in fig.2(a). Sensor pods are arranged along each of the sensor booms. The booms are mounted to a moveable carriage which is carried up the column by a linear actuator. The booms are extended and retracted by a linear actuator at the base of the sensor boom. Motion of this actuator, combined with motion of the carriage linear actuator, permits the booms to deploy while maintaining constant boom tip-to-ground distance. This substantially horizontal motion of the boom tip permits the sensor booms to enter the plant rows without damage to the plants. Once fully deployed the carriage linear actuator moves the booms upwards along the column to scan plants. After reaching the top of the scan, booms are retracted in reverse of the deployment motion and the system is moved to the next plant row to be scanned. The deployment sequence is depicted in fig.2(b). The system operates at the rate of 72 plants/hour which is much higher than the manual methods.

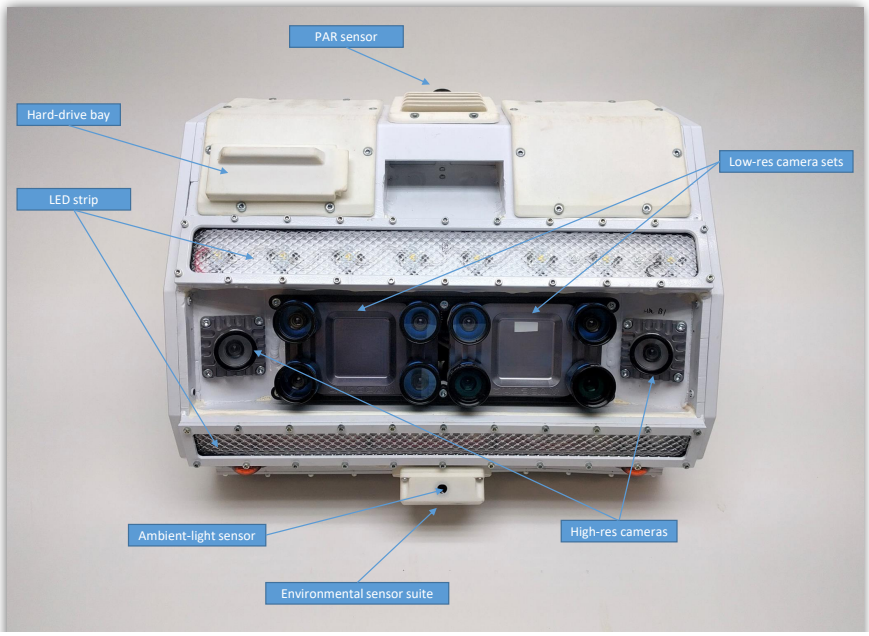

Fig. 3: Sensorpod - Sensing module integrated with 10 cameras, environmental sensors, computing and storage

3.1 Sensorpod

The sensorpod has 10 cameras with 8 (low resolution) cameras placed in two rows and remaining 2 (high resolution) cameras to the sides at a verged angle of 30 degrees. The cameras are hardware synchronized and triggered every 10 cms when the boom moves up the canopy. The top center pair cameras are designated for stereo reconstruction. The other low-resolution cameras carry narrow bandpass filters to capture images in multiple wavelengths. 450nm and 550nm filters correspond to the chlorophyll absorption bands 2 and 3, the 740nm and 940nm filters correspond to the normalized difference vegetation index and 950nm filter correspond to nitrogen band. The high-resolution verged cameras are used for Structure-from-Motion reconstructions. A bright LED strip with diffusers is located below the camera array so as to provide uniform illumination inside densely covered plant canopies. An ambient light sensor is attached to the bottom of the sensorpod, looking at the plant, to help set the exposure values of the cameras. A PAR [1] sensor is mounted on top of the sensorpod to make photosynthetic light measurements when the system moves along the canopy. There is also an environmental sensor suite which measures the temperature, humidity and CO_2 mounted inside the sensorpod. All the cameras and

[1] PAR - Photosynthetically Active Radiation is the spectral range of the solar radiation that plants use during photosynthesis

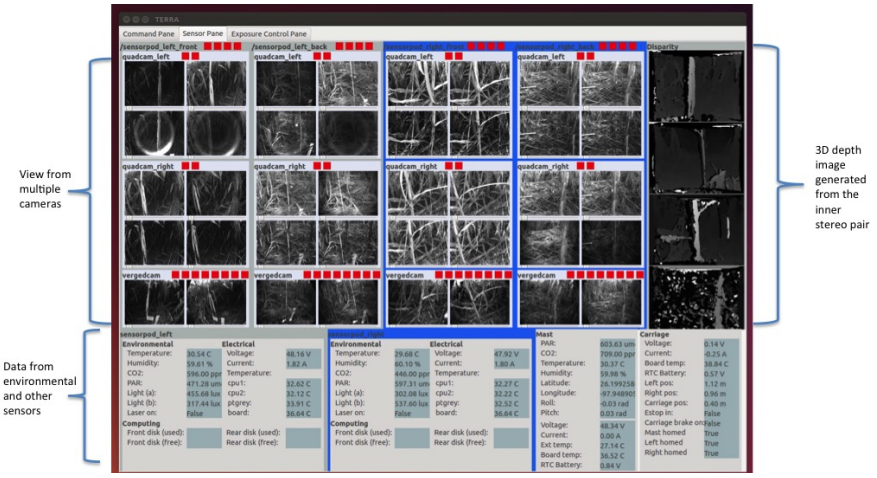

Fig. 4: User interface showing the camera view. The top section streams camera data from the different cameras along with a 3d depth image generated using the top inner stereo pair cameras. The bottom section shows the data streaming from the environmental and other sensors.

sensors are connected to a embedded computer (Intel i7 3.4GHz) running Ubuntu 14.04. In addition to the internal storage, a 1TB SSD is connected to the computer exclusively for data logging. An identical setup, with the cameras and computer is mounted on the other side of the sensorpod so that the system can scan two rows simultaneously. Since most LiDAR units do not provide high spatial resolution or close range ($<$10cm), we do not use LiDAR for the purpose of dense 3D reconstruction of plants.

3.2 Data Collection and Interface

The robotic system has 2 sensorpods on either side and can scan 4 plants in one sweep. The design supports 8 or 12 sensorpods in total. This results in data flowing through 40 cameras and other environmental sensors simultaneously. In order to achieve this throughput, the data is logged locally as noted in the previous section. This gives us the freedom to add sensorpods to the boom without worrying about bandwidth issues. We still need to monitor the data from all the sensors including cameras and make sure it is logged properly. We accomplish this using the software architecture proposed in Fig. 4.

The *health and status* process monitors the health of all the processes running on the computer and also pulls images from the camera driver and sends image thumbnails and histograms to the *user interface (UI)* built using the Robot Operating System (ROS) framework. So if any camera fails, or if the image is not good (over/under exposed, foreground not in focus, etc) the operator can work on it. The

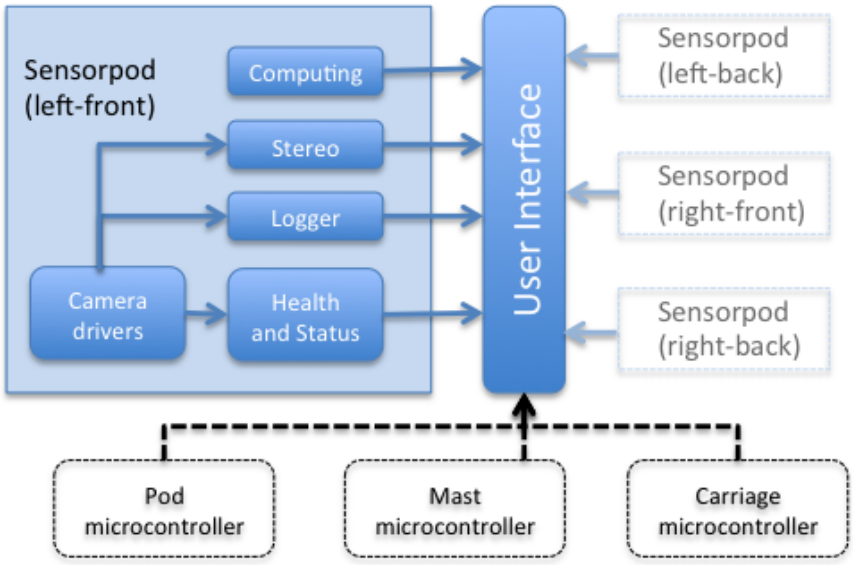

Fig. 5: Software architecture - The camera drivers feed image data to the different processes which in-turn feed their status to the user interface. An identical version of the software suite runs on each of the sensorpods. The encoder positions and other system level information flows from the micro-controllers to the user interface

logger stores full resolution images from the camera drivers locally. After a scan is completed, the *logger* reports the number of frames logged to the *UI* so that dropped frames are noted immediately. The *computing* process monitors the state of the computer and sends vital information to the UI for tracking and monitoring. The *stereo* process generates disparities from the stereo pair and pushes them to the *UI* for inspection. A clone of similar processes run on all the sensorpod computers which talk to the central UI component. Fig. 5 shows a snapshot of the UI with data streaming from the four sensorpod computers. It is crucial that we properly localize the robot so that the logs are tagged appropriately. To help on that front, the user interface displays a table of the plot layout and the operator would click on which plot the robot is scanning.

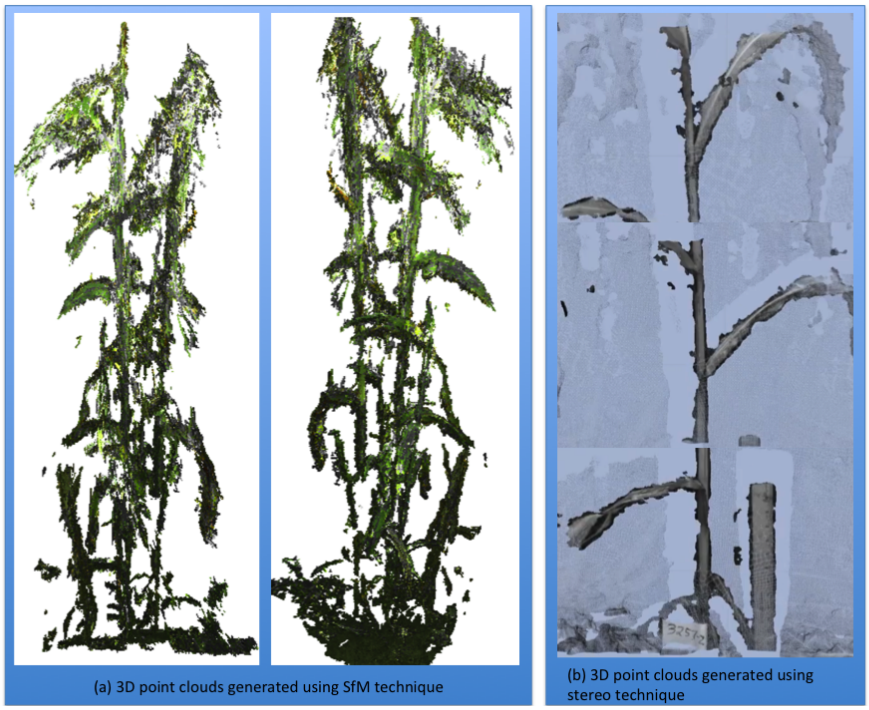

Fig. 6: 3D point cloud of Sorghum plant generated using (a) SfM technique (b) using stereo (SGBM) method

4 Modeling Plants

4.1 3D Reconstruction

Structure from Motion (SfM): Structure from Motion uses 2D grayscale images from different view-points to construct a point cloud of the scene. It takes in rectified images, finds features in the images and matches them. It then triangulates these feature matches to obtain 3D point positions using an initial estimate of the camera pose. The camera pose constituting intrinsics and extrinsics along with the 3D point positions are then collectively solved for in an optimization problem that seeks to minimize overall reprojection error [15], [16] . This gives a sparse point cloud which is then fed to a patch-growing algorithm like [5] to create a dense point cloud of the scene. An example of the point cloud constructed using SfM technique[15], [16] is shown in fig.6(a). Using SfM techniques we can reconstruct the full plant model. The reconstructed plant model is geometrically consistent as it uses images from multiple known viewpoints.

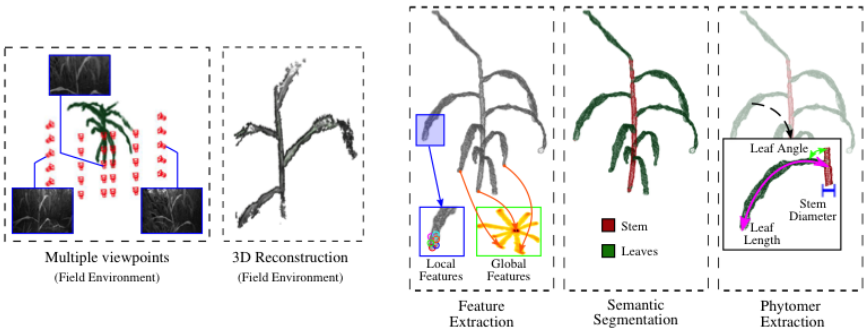

Fig. 7: Automated pipeline mapping input plant images to segmented 3D phytomer units. The first two modules take plant images captured from multiple viewpoints and generate a 3D point cloud reconstruction of the plant. Once the 3D reconstruction is obtained, local and global 3D point features are extracted. The next module uses a machine learning classifier to assign a semantic class label to each 3D point. Finally, the phytomer is extracted from the segmented point cloud.

Stereo: For stereo point clouds we can only use the images from the inner pair of cameras on the top row. Since the plants are real close to the cameras (35-55 cms), using any other camera will make the disparity too big to be usable. Stereo reconstruction generally produces denser point clouds, but compared to the point clouds from SfM reconstruction, they are not as geometrically consistent as it uses fewer images and limited view-points. Also, this technique produces point clouds for each pair of frames and they have to be stitched (using techniques like Iterative Closest Point [6]) to generate the full 3D model. Figure 6(b) shows a 3d point cloud generated using stereo reconstruction technique.

4.2 Segmentation and Phytomer Extraction

A phytomer unit is a functional building block for the plant which consists of a leaf, its sheath and the stem segment on which the leaf resides. The pipeline[23] mapping input plant images to 3D phytomers is illustrated in Fig. 7. The first stage illustrates the generation of 3D point cloud from images. The next step computes point-level 3D features [10] using local geometries and a global distance metric to density modes. Each point is then classified as a stem or a leaf by learning a Support Vector Machine decision boundary, followed by spatial smoothing using a Conditional Random Field [11]. Next, the semantic segmentation step classifies each 3D point into one of two semantic classes, stem and leaf. The phytomer extraction step proceeds by performing RANSAC fit of a 3D cylinder model [8] to the points labeled as stem. The fitted cylinder is then expanded by $\sim$25% to intersect leaves branching out from the stem. Each intersection point, referred to as a node, is then passed as a seed point to a region growing algorithm [9] so as to extract a single leaf

growing from that node. Once individual leaves at each of the nodes are extracted, these are then merged with a section of stem around the node to obtain a phytomer unit corresponding to that particular node.

5 Estimating Phenotypes

Since the field data is noisy due to occlusion, wind, etc, pure geometric approaches like surface fitting perform badly for phenotype estimation. Instead, we build a neural network model for this task. To be specific, the segmented phytomers are first binned into voxels. The voxels are then fed to the neural network for prediction. However, because the number of segmented phytomers are limited, the neural network cannot make good predictions if it is trained on real data alone. To alleviate this problem, we simulated plants based on the model from botanists and use this synthesized data set to train our model. We use the Multilayer Perceptron architecture with 4 hidden layers. The sizes of the layers are 5000, 1000, 200, 100. The plant point clouds are binned into voxels with dimension $30 \times 20 \times 50$. We serialize the $30 \times 20 \times 50$ voxels into vectors of size 30,000 before feeding them to the neural network. The neural network is trained on 10,000 synthesized plants with dropout probability 0.8 and learning rate 0.0001.

6 Field Experiments and Observations

We deployed a prototype in Puerto Rico in February 2016 to gain insights at the needs and challenges in designing the sensorpod. In October 2016 we deployed the robotic system in College Station, Texas and again in December 2016 in Weslaco, Texas.

6.1 Exposure Control

Camera exposure control is critical to obtaining high-quality data in this environment of dappled constantly changing lighting. Our system utilized light sensing to set camera exposure, as auto-exposure control algorithms were not feasible with our low frequency trigger-based capture process. The dynamic range of our scenes gradually increased along with required exposure time from the top of the plant moving downwards to the bottom of the plant creating dissimilarities in ideal exposure values. The varying relative intensities between ambient light and LED arrays as we moved from the top to the bottom, introduced a non-linearity to light-exposure relation. If images were under or over exposed, features would become indistinguishable in the image, underlining the importance of this process. In order to tackle

this issue, we tried the following techniques, however, the problem is not solved completely. (a) We used the high dynamic range (HDR) setting procedure to aid in compressing the dynamic range of the scene into a capturable image. (b) We incorporated brighter LED arrays into the sensorpod to increase the illumination at the bottom section of the plants. At the top of the canopy though, it couldn't be contrasted to the much brighter sunlight. (c) We used the ambient light sensor and PAR sensor on the sensorpod and mast, to set exposure of the cameras. Exposure controllers for the stereo camera were first calibrated to the light sensors. This was done in the field, using images of the scene at different heights so as to correctly expose the plants which covered most of the scene, while still keeping the brightest and darkest spots of the dynamic range unsaturated. An 18% gray card was used as a middle-gray reference to seed calibration. The resulting light-exposure relationship is given by:

$$exposure = K/(light)$$

where K is the calibration constant. Therefore, doubling the light (increasing by one stop), would halve the exposure. Finally, offsets were calculated experimentally for the filtered imagers based off the relative intensities of solar radiation in the narrow wavelength bands. During field tests due to non-linearities mentioned earlier, we had to periodically adjust calibration thresholds based on the time of the day and cloud cover.

Though the current illumination helped at bottom of canopy, the imaging system needs much more illuminated light to fully subtract the ambient sunlight above about 500 $\mu mol/m^2/s$ [2]. Night scans with illumination yielded datasets with good amount of background subtraction which helped the plant modeling algorithms.

6.2 Field of View (FOV)

It was quickly established that the wider FOV lens was not ideal from many aspects. The wide FOV lens accepted light that the multispectral filters could not consistently block. Filters only function with a certain angle of incidence (AOI) of light, but the lens captured light outside of that region, which corresponded with a rainbow effect in the images.

Other problems with the wide field of view lens were pixel density (resolution) and depth of field related. A wider field of view lens would require a higher resolution imager to maintain the pixel density, which would increase the computing system demand from acquisition, to storage, to processing.

The depth of field of a lens in this relatively close imaging arrangement is significantly reduced when compared to the same lens focused at its hyperfocal distance. This problem is exacerbated with a wide field of view lens, where the distance a subject is from the lens varies greatly from the center of the image to the ends.

[2] $\mu mol/m^2/s$ is based on the number of photons in a certain waveband incident per unit time on a unit area divided by the Avogadro constant

These concerns lead us to compromise on the amount of a row in view per camera, to obtain better image quality.

In our prototypes we used a lens with larger aperture f/2.6. But the depth of field was too shallow and we switched to a smaller aperture (f/4.0) lens. This yielded a larger depth of field at the expense of less light reaching the image sensor.

6.3 Filters

The commercially available off the shelf filters did not perform as expected. Some of the filters were reflective and applied to thick substrates while not evenly blocking light though the required FOV. This produced artifacts in the image. There also seemed to be a signal to noise component to this artifact. It was most notable in the filters for the 940 and 950nm wavelengths where there isn't much sunlight due to water vapor absorption in the atmosphere, which reduced the filter efficiency.

6.4 Ground Truth

Taking ground truth measurement and associating the measurements to the robot collected imagery is a manually intensive and error prone process. For instance consider the leaf angle measurement process. The leaf angle phenotype generally refers to the first leaf below the flag leaf (top leaf). This leaf could have tillers coming out of the node. Tiller is a side shoot emanating from the main stem. Even for a keen human observer, the process of distinguishing a leaf from a tiller can be confusing. Assuming the distinction is made and the leaf angle measured, they need to be identified precisely from robot obtained imagery. This should be straight forward if we have the full 3D plant reconstruction. To tackle this problem, we tagged leaves for which we took ground truth leaf angle measurements. The tagging was done by tying a bright colored ribbon below the leaves. During post processing, the tag detection was automated and the manual measurements were then associated to the robot-collected data.

7 Results and Analysis

We scanned 991 fully grown sorghum plants using this system of which 170 plants were ground truthed. The ground truth phenotype measurements included leaf angle, stem diameter, leaf area and plant height.

Fig. 8 shows qualitative results for phytomer extraction on the field data collected in Dec 2016. It shows the semantically segmented point cloud followed by CRF smoothing along with the extracted 3D phytomers.

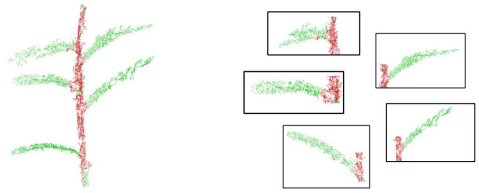

(a) (b)

Fig. 8: (a) shows qualitative segmentation outputs from SVM followed by CRF smoothing for field environment. (b) shows segmented 3D phytomers extracted from the plant point cloud in (a).

While the field data was processed and the segmentation algorithms were developed, we scanned the plants using a RGB-D sensor (indoors) and tested our neural network implementation. The neural network was trained on 10,000 synthesized plants with dropout probability 0.8 and learning rate 0.0001. The trained model was evaluated on 54 real plants to either predict phenotype values or determine whether the value is greater or smaller than the median value of all those real plants. Table.1 shows the predicted phenotypes along with their root mean squared errors relative to the range of the phenotype. Our current result is better than the naively using the mean all of data for prediction. The result can be improved in the future by passing the voxels into a CNN without serialization, increasing the resolution (number of voxels used) and adopting transfer learning techniques.

Phenotype	**Relative root mean squared error (%)**
Leaf Area	26.15
Leaf Length	26.67
Leaf Width	25.15

Table 1: Relative root mean squared error on plant phenotypes measured using RGB-D sensor

8 Conclusion

We presented a high-throughput non-intrusive phenotyping robot that takes multiple phenotypic measurements throughout the life of the crop with minimal human intervention. It is designed to handle the high volume data and make phenotypic measurements. Through field validation of the system and the observations focused on bioenergy sorghum, the technology is deployable to a range of biomass crops as well as agronomic row crops.

References

1. E. J. Araus, Jos Luis , Cairns, "Field high-throughput phenotyping: the new crop breeding frontier," Trends Plant Science., vol. 19, no. 1, pp. 52-61, 2014.
2. N. Fahlgren, M. A. Gehan, and I. Baxter, "Lights, camera, action: High-throughput plant phenotyping is ready for a close-up," Curr. Opin. Plant Biol., vol. 24, pp. 93-99, 2015.
3. Mullet, J., D. Morishige, R. McCormick, S. Truong, J. Hilley, B. McKinley, R. Anderson, S.N. Olson, W. Rooney. 2014. Energy sorghum–a genetic model for the design of C4 grass bioenergy crops, Journal of experimental botany, 65:3479-3489.
4. Vermerris W. 2011. Survey of genomics approaches to improve bioenergy traits in maize, Sorghum and sugarcane. Journal of Integrative Plant Biology 53, 105-119.
5. Yasutaka Furukawa and Jean Ponce Accurate, Dense, and Robust Multi-View Stereopsis IEEE Transactions on Pattern Analysis and Machine Intelligence, Vol. 32, Issue 8, Pages 1362-1376, August 2010.
6. P. Besl and N. McKay. A method for registration of 3D shapes. IEEE Transactions on Pattern Analysis and Machine Intelligence (PAMI), 14(2):239 - 256, 1992.
7. R. F. Mccormick, S. K. Truong, and J. E. Mullet. 3d sorghum recon- structions from depth images identify qtl regulating shoot architecture. Plant Physiology, pages pp - 00948, 2016.
8. Schnabel, Ruwen, Roland Wahl, and Reinhard Klein. "Efficient RANSAC for pointcloud shape detection." Computer graphics forum. Vol. 26. No. 2. Blackwell Publishing Ltd, 2007.
9. Rusu, Radu Bogdan, and Steve Cousins. "3d is here: Point cloud library (pcl)." Robotics and Automation (ICRA), 2011 IEEE International Conference on. IEEE, 2011.
10. Rusu, Radu Bogdan, Nico Blodow, and Michael Beetz. "Fast point feature histograms (FPFH) for 3D registration." Robotics and Automation, 2009. ICRA'09. IEEE International Conference on. IEEE, 2009.
11. Koltun, Vladlen. "Efficient inference in fully connected crfs with gaussian edge potentials." Adv. Neural Inf. Process. Syst 2.3 (2011): 4.
12. Li, Lei, Qin Zhang, and Danfeng Huang. "A review of imaging techniques for plant phenotyping." Sensors 14.11 (2014): 20078-20111.
13. Weiss, Ulrich, and Peter Biber. "Plant detection and mapping for agricultural robots using a 3D LIDAR sensor." Robotics and autonomous systems 59.5 (2011): 265-273.
14. Slaughter, D. C., D. K. Giles, and D. Downey. "Autonomous robotic weed control systems: A review." Computers and electronics in agriculture 61.1 (2008): 63-78.
15. C. Wu, "Towards linear-time incremental structure from motion," Proc. - 2013 Int. Conf. 3D Vision, 3DV 2013, pp. 127-134, 2013.
16. S. Fuhrmann, F. Langguth, and M. Goesele, "MVE-A Multi-View Reconstruction Environment," Eurographics Workshops on Graphics and Cultural Heritage, 2014.
17. Dey, Debadeepta, Lily Mummert, and Rahul Sukthankar. "Classification of plant structures from uncalibrated image sequences." Applications of Computer Vision (WACV), 2012 IEEE Workshop on. IEEE, 2012. APA
18. Lehnert, Christopher, et al. "Autonomous sweet pepper harvesting for protected cropping systems." IEEE Robotics and Automation Letters 2.2 (2017): 872-879.
19. Chaivivatrakul, Supawadee, et al. "Automatic morphological trait characterization for corn plants via 3D holographic reconstruction." Computers and Electronics in Agriculture 109 (2014): 109-123.
20. Ribera, Javier, et al. "Estimating Phenotypic Traits From UAV Based RGB Imagery."
21. Virlet, Nicolas, et al. "Field Scanalyzer: An automated robotic field phenotyping platform for detailed crop monitoring." Functional Plant Biology 44.1 (2017): 143-153.
22. Bangert, Waldemar, et al. "Field-robot-based agriculture: RemoteFarming and BoniRob-Apps" VDI-Berichte 2193 (2013): 439-446.
23. P. Sodhi, S. Vijayarangan, and D. Wettergreen, "In-field Segmentation and Identification of Plant Structures using 3D Imaging," IEEE/RSJ International Conference on Intelligent Robots and Systems 2017.